

## Scattering Cross Sections for Electron Transport Using Energy-Finite-Element Weighting

Clif Drumm and Ronald P. Kensek

*Radiation Effects Theory Dept.*

*Sandia National Laboratories<sup>a</sup>, PO Box 5800, Albuquerque, NM 87185-1179*

[crdrumm@sandia.gov](mailto:crdrumm@sandia.gov)

**Abstract** – A method is described for computing scattering cross sections that are weighted by energy-finite-element (FE) basis functions, as an alternative to traditional multigroup. The weighted cross sections are needed for transport codes that use energy-FE for handling the energy dependence of the Boltzmann transport equation. The method is applied to electron inelastic scattering, where steep gradients in the cross-section energy dependence may make a multigroup treatment problematic. For electron scattering, a continuous-slowning-down (CSD) model is used for small energy-loss events in conjunction with a Boltzmann treatment for larger-energy-loss events. An electron inelastic scattering model is used to compute stopping powers that are compared with experimental values. Energy-FE weighted cross sections are used in several method-of-manufactured-solutions (MMS) test problems to demonstrate the validity of the cross sections and to show convergence with energy-mesh refinement.

### I. INTRODUCTION

Electron scattering is extremely forward peaked, and the cross sections vary rapidly with energy, so that a Multi-Group-Legendre (MG-L) energy/angular treatment introduces error which is difficult to characterize. Using an Energy-Finite-Element (FE) approximation, rather than MG, results in a more-accurate characterization of the electron transport. Developing group-to-group scattering cross sections for energy-FE requires energy integrations of cross sections and stopping powers weighted by energy basis functions, as will be described.

A multi-year effort has begun to replace the legacy Coupled Electron Photon Cross Section (CEPXS) code [1, 2] which has been widely used to generate MG-L electron/photon/positron cross sections for use by deterministic and MG Monte Carlo transport codes, with a new C++ code with a number of improvements, including the production of energy-FE weighted cross sections and stopping powers. The use of a single “step” energy basis function for weighting the cross sections results in standard MG cross sections.

Another improvement in the generation of electron cross sections will be to provide a flexible partition between Continuous Slowing Down (CSD) (small energy loss and deflection) and “catastrophic” (large energy loss and deflection) scattering treatments. In the current CEPXS code, scattering to an adjacent group is treated by CSD and scattering beyond an adjacent group (so-called “catastrophic” scattering) is treated by a standard MG-L approximation. The new code will allow for an arbitrary partition between CSD and MG-L treatments, specifying either a specific energy loss or specific angular deflection to demark the CSD and catastrophic-scattering treatments. Finally, the new code will have the capability of generating cross sections below the current minimum of 1 keV and use more accurate scattering models.

### II. BACKGROUND

Electron transport is characterized by extremely forward peaked angular dependence and rapidly varying cross-section and stopping-power dependence with energy, making a MG-L energy/angular approximation difficult. Using energy-FE rather than MG results in a more-accurate approximation with easier-to-characterize error. Parallel efforts are underway to productize energy-FE capability in the SCEPTRE radiation transport code [3] and to develop a replacement to the legacy CEPXS [1] code that will provide energy-FE cross sections and stopping powers.

Two distinct methods are used to handle the extreme forward-peaked scattering cross section dependence, 1) the CSD approximation and 2) the  $\delta$ -down-scatter approximation [4]. In the CSD approximation, either a specific energy loss or a specific scattering angle is specified to demark the portion of the scattering handled by CSD and that handled by a standard MG-L approximation. In this manner, a restricted stopping power is computed that includes only the most forward-peaked portion of the scattering, neglecting angular deflection, and “catastrophic” scattering that includes both energy loss and angular deflection which are handled by a standard MG-L approximation.

The  $\delta$ -down-scatter approximation is applied to the MG-L by separating out a  $\delta$ -function in angle term from the MG-L down-scatter cross section moments, resulting in much less anisotropic scattering moments [4]. Both the CSD and  $\delta$ -function approximations have a similar effect, that of reducing particle energy without direction change, but numerical behavior is quite different.

In the following section, the energy-FE formulation of the Boltzmann equation will be described, including both the CSD treatment and the  $\delta$ -down-scatter approximation. Then, a particular form of the electron inelastic scattering cross section, the Relativistic Binary Encounter Dipole (RBED) cross section [5], will be described and used to

compute stopping powers. These will be compared with experimental values, followed by the results of several Method of Manufactured Solutions (MMS) test problems to demonstrate the validity of the cross sections and to show convergence with energy-mesh refinement. For simplicity, all of the test problems presented are one-dimensional in space. However, there is nothing to prevent the energy-FE weighted cross sections from also being used in multi-dimensional problems.

### III. ENERGY FE-WEIGHTED CROSS SECTIONS

The Boltzmann transport equation is

$$\mathbf{\Omega} \cdot \nabla \psi + \sigma_t \psi(\mathbf{r}, \mathbf{\Omega}, E) = Q(\mathbf{r}, \mathbf{\Omega}, E) + \int_E^{E_{\max}} \int_{4\pi} \sigma_s(\mathbf{\Omega}' \rightarrow \mathbf{\Omega}, E' \rightarrow E) \psi(\mathbf{r}, \mathbf{\Omega}', E') d\mathbf{\Omega}' dE', \quad (1)$$

where  $\mathbf{r}$ ,  $\mathbf{\Omega}$  and  $E$  are the spatial position, direction of motion, and energy, respectively, and  $E_{\max}$  is the global upper-energy limit. The energy limits of integration assume no upscatter.  $\psi$  is the angular flux and  $Q$  is a source term, and  $\sigma_s$  is the scattering cross section. The scattering cross section may be written in terms of  $\mu_0$ , the cosine of the angle between the pre- and post-scattered direction of motion,

$$\sigma_s(\mathbf{\Omega}' \rightarrow \mathbf{\Omega}, E' \rightarrow E) = \frac{1}{2\pi} \sigma_s(\mu_0, E' \rightarrow E), \quad (2a)$$

and integrating over angle results in the energy scattering cross section,

$$\sigma_s(E \rightarrow E') = \int_{-1}^1 \sigma_s(\mu_0, E \rightarrow E') d\mu_0. \quad (2b)$$

The stopping power may be computed from

$$S(E) = \int_{E/2}^E (E - E') \sigma_s(E \rightarrow E') dE'. \quad (3)$$

The lower integration limit is  $E/2$  since, in an inelastic electron-electron collision, two electrons emerge, and by convention, the higher-energy scattered electron is considered the primary and the lower-energy scattered electron is considered a secondary.

The restricted stopping power,  $S_R$ , is computed by specifying a maximum energy loss,  $\Delta$ , to be included in the restricted stopping power

$$S_R(E) = \int_{E-\Delta}^E (E - E') \sigma_s(E \rightarrow E') dE'. \quad (4)$$

The Boltzmann-CSD equation may then be written as

$$\mathbf{\Omega} \cdot \nabla \psi + \sigma_t \psi(\mathbf{r}, \mathbf{\Omega}, E) - \frac{\partial(S_R \psi)}{\partial E} = Q(\mathbf{r}, \mathbf{\Omega}, E) + \int_{E+\Delta}^{E_{\max}} \int_{4\pi} \sigma_s(\mu_0, E' \rightarrow E) \psi(\mathbf{r}, \mathbf{\Omega}', E') d\mathbf{\Omega}' dE'. \quad (5)$$

The catastrophic scattering is expanded in Legendre moments

$$\sigma_{sl}(E' \rightarrow E) = \int_{-1}^1 P_l(\mu_0) \sigma_s(\mu_0, E' \rightarrow E) d\mu_0, \quad (6a)$$

resulting in an approximation of the angle/energy scattering cross section of

$$\sigma_s(\mu_0, E' \rightarrow E) \cong \sum_{l=0}^L (2l+1) P_l(\mu_0) \sigma_{sl}(E' \rightarrow E). \quad (6b)$$

With the  $\delta$ -down-scattering cross section removed, the scattering moments are

$$\tilde{\sigma}_{sl}(E' \rightarrow E) \equiv \sigma_{sl}(E' \rightarrow E) - \sigma_{sL}(E' \rightarrow E), \quad (7a)$$

resulting in an approximation of the catastrophic scattering of

$$\sigma_s(\mu_0, E' \rightarrow E) \cong \sum_{l=0}^{L-1} (2l+1) P_l(\mu_0) \tilde{\sigma}_{sl}(E' \rightarrow E) + (2L+1) \sigma_{sL}(E' \rightarrow E) \delta(1 - \mu_0). \quad (7b)$$

The Boltzmann-CSD equation with  $\delta$ -down-scatter is

$$\mathbf{\Omega} \cdot \nabla \psi + \sigma_t \psi(\mathbf{r}, \mathbf{\Omega}, E) - \frac{\partial(S_R \psi)}{\partial E} = Q(\mathbf{r}, \mathbf{\Omega}, E) + \sum_{l,m} Y_{l,m}(\mathbf{\Omega}) \int_{4\pi} Y_{l,m}(\mathbf{\Omega}') \int_{E+\Delta}^{E_{\max}} \tilde{\sigma}_{sl}(E' \rightarrow E) \psi(\mathbf{r}, \mathbf{\Omega}', E') dE' d\mathbf{\Omega}' + (2L+1) \int_{E+\Delta}^{E_{\max}} \sigma_{sL}(E' \rightarrow E) \psi(\mathbf{r}, \mathbf{\Omega}, E') dE', \quad (8)$$

with the  $2l+1$  factors included in the spherical harmonics functions.

Applying an energy-FE approximation is done by expanding the angular flux in energy basis functions and expansion coefficients

$$\psi(\mathbf{r}, \mathbf{\Omega}, E) \cong \sum_i \psi_g^i(\mathbf{r}, \mathbf{\Omega}) \phi_g^i(E), \quad E \in [E_{g,l}, E_{g,u}], \quad (9a)$$

where  $\phi_g^i(E)$  are the energy basis functions for energy element (energy group)  $g$  and energy basis function  $i$ , and  $\psi_g^i(\mathbf{r}, \mathbf{\Omega})$  are the expansion coefficients as a function of space and angle.  $E_{g,l}$  and  $E_{g,u}$  are the lower and upper energy bounds, respectively, of the energy element (group). For example, linear energy basis functions are

$$\phi_g^1(E) = \frac{E_{g,u} - E}{\Delta E_g}, \quad E \in [E_{g,l}, E_{g,u}] \quad (9b)$$

and

$$\phi_g^2(E) = \frac{E - E_{g,l}}{\Delta E_g}, \quad E \in [E_{g,l}, E_{g,u}]. \quad (9c)$$

The weak form of the Boltzmann-CSD equation is obtained by substituting the expression for the angular flux, Eq. (9a), into Eq. (8), multiplying by an energy basis function, integrating over  $E$  and integrating the CSD term by parts, resulting in a discontinuous-FE (DFE) formulation

$$\begin{aligned}
 & \sum_{i'} [\mathbf{\Omega} \cdot \nabla \psi_g^{i'} \langle \varphi_g^i(E), \varphi_g^{i'}(E) \rangle + \psi_g^{i'}(\mathbf{r}, \mathbf{\Omega}) \langle \varphi_g^i(E), \sigma_t(E) \varphi_g^{i'}(E) \rangle \\
 & + \psi_g^{i'}(\mathbf{r}, \mathbf{\Omega}) \left\langle \frac{d\varphi_g^i}{dE}, S_R(E) \varphi_g^{i'}(E) \right\rangle] + S_R(E_{g,l}) \psi_g^{i'}(\mathbf{r}, \mathbf{\Omega}) \\
 & = S_R(E_{g-1,l}) \psi_{g-1}^{i'}(\mathbf{r}, \mathbf{\Omega}) + \sum_{i'} [Q_g^{i'}(\mathbf{r}, \mathbf{\Omega}) \langle \varphi_g^i(E), \varphi_g^{i'}(E) \rangle \\
 & + \sum_{l,m} Y_l^m(\mathbf{\Omega}) \int_{4\pi} Y_l^m(\mathbf{\Omega}') \sum_{g'} \psi_{g'}^{i'}(\mathbf{r}, \mathbf{\Omega}') \\
 & \langle \varphi_g^i(E), \langle \sigma_{sl}(E' \rightarrow E), \varphi_{g'}^{i'}(E') \rangle \rangle d\mathbf{\Omega}' \\
 & + (2L+1) \sum_{g'} \psi_{g'}^{i'}(\mathbf{r}, \mathbf{\Omega}) \langle \varphi_g^i(E), \langle \sigma_{sl}(E' \rightarrow E), \varphi_{g'}^{i'}(E') \rangle \rangle] \cdot (10)
 \end{aligned}$$

Energy-FE weighted stopping powers

$$S_{R,g}^{i,i'} = \left\langle \frac{d\varphi_g^i}{dE}, S_R(E) \varphi_g^{i'}(E) \right\rangle \quad (11a)$$

and scattering cross sections

$$\sigma_{sl,g \rightarrow g'}^{i,i'} = \langle \varphi_g^i(E), \langle \sigma_{sl}(E' \rightarrow E), \varphi_{g'}^{i'}(E') \rangle \rangle \quad (11b)$$

are computed by the cross-section processing code by using an adaptive integration routine.

In order to test the validity of the energy-FE weighted cross sections, a particular form of the inelastic electron-electron scattering kernel is chosen. The Relativistic Binary Encounter Dipole (RBED) differential scattering cross section is [5]

$$\begin{aligned}
 \sigma_{RBED}(E \rightarrow E') & = \sum_j \frac{4 \cdot 10^{24} \pi a_0^2 \alpha^4 Z_j m_0 c^2 N}{(\beta_i^2 + \beta_u^2 + \beta_b^2) b_j^2} \\
 & \left\{ \frac{4m_0 c^2 (2E + m_0 c^2) b_j^2}{(E + 2m_0 c^2)^2 (E - E')(E' + b_j)} \right. \\
 & + \frac{b_j^2}{(E - E')^2} + \frac{b_j^2}{(E' + b_j)^2} + \frac{4b_j^2}{(E + 2m_0 c^2)^2} \\
 & + \frac{b_j^3}{(E' + b_j)^3} \left[ \ln \left( \frac{E(E + 2m_0 c^2)}{(m_0 c^2)^2} \right) \right. \\
 & \left. \left. - \frac{E(E + 2m_0 c^2)}{(E + m_0 c^2)^2} - \ln \left( \frac{2b_j}{m_0 c^2} \right) \right] \right\}, \quad (12a)
 \end{aligned}$$

where  $a_0$  is the Bohr radius,  $\alpha$  is the fine-structure constant,  $Z_j$  is the occupancy of level  $j$ ,  $m_0 c^2$  is the electron rest mass,  $N$  is the number density of the material, and  $b_j$  is the binding energy of the level.  $\beta_i^2 + \beta_u^2 + \beta_b^2$  plays the role of the focusing factor, as described in Ref. [5]. Kinetic and binding energies for use in Eq. (12a) are obtained from the Lawrence Livermore National Laboratory (LLNL) database [6].

Eq. (12a) was obtained from Kim, et al. (Ref. [5]) by introducing a couple of approximations to Kim's RBED

model. Starting from Kim et al. Eq. (19), the BEQ simplification is introduced,

$$\left( \frac{df}{dw} \right)_{BEQ} = \frac{N_i}{(w+1)^2}, \quad (12b)$$

which is Kim et al. Eq. (7). Furthermore, the Binary-Encounter-Bethe (BEB) simplification [5] is introduced by setting

$$\frac{N_i}{N} = 1. \quad (12c)$$

Fig. 1 shows the RBED differential scattering cross section for gold from 0.1 MeV to scattered electron energies down to 1 keV, showing the extreme energy dependence of the cross section for near-zero energy loss and for small scattered electron energy.

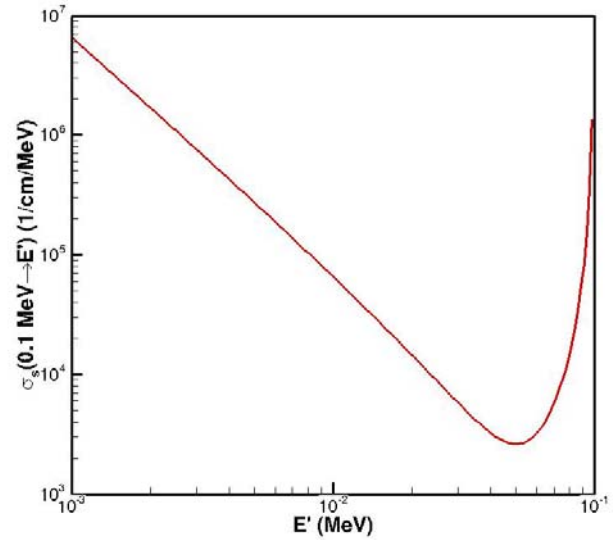


Fig. 1. RBED differential scattering cross section for gold, illustrating the extreme dependence of the cross section with energy.

From the relativistic scattering kinematics, the cosine of the angle between the source electron and primary scattered electron (neglecting the shell binding energy) is

$$\mu_0(E \rightarrow E') = \frac{\sqrt{E'(E + 2m_0 c^2)}}{\sqrt{E(E' + 2m_0 c^2)}}, \quad (13a)$$

resulting in the fully-differential scattering cross section

$$\sigma_{RBED}(\mu_0, E \rightarrow E') =$$

$$\delta \left( \mu_0 - \frac{\sqrt{E'(E + 2m_0 c^2)}}{\sqrt{E(E' + 2m_0 c^2)}} \right) \sigma_{RBED}(E \rightarrow E'), \quad (13b)$$

with scattering moments given by

$$\sigma_l(E \rightarrow E') = P_l \left( \frac{\sqrt{E'(E + 2m_0 c^2)}}{\sqrt{E(E' + 2m_0 c^2)}} \right) \sigma_{RBED}(E \rightarrow E'). \quad (13c)$$

As a test of the validity of the RBED cross section model, the RBED cross section can be used to compute stopping powers that can be compared with experimental values. Because the RBED cross section contains a singularity in the limit of zero energy loss, the upper integration limit in Eq. (3) must be truncated to some value less than the primary electron energy. It would seem that reasonable lower and upper integration limits for Eq. (3) would be  $(E - b_j)/2$  and  $E - b_j$ , respectively, where  $b_j$  is the binding energy of the level. It turns out, however, that better agreement with experimental stopping-power values for aluminum and gold are obtained by using lower and upper integration limits of  $E/2$  and  $E - b_j/2$ , resulting in a stopping power computed from,

$$S(E) \equiv \sum_j Z_j \int_{E/2}^{E - b_j/2} (E - E') \sigma_{RBED,j}(E \rightarrow E') dE', \quad (14)$$

where  $\sigma_{RBED,j}$  is the portion of the RBED cross section for energy level  $j$ . Calculated stopping powers tend to be quite sensitive to the limits chosen for the energy integrations. This warrants further investigation.

Kinetic and binding energies for aluminum and gold for use in Eqs. (12a) and (14) are obtained from the LLNL database [6]. Fig. 2a. shows a comparison of the aluminum stopping power computed using the RBED differential scattering cross section with NIST data [7] and experimental values from the Joy database [8]. The Joy references refer to the references in the Joy report [8]. The RBED values are obtained from Eq. (14) by applying an adaptive integration routine to perform the energy integral. The agreement is very good for electron energies down to 20 eV with the Joy Ref. 89 data, using  $E - b_j/2$  as an upper bound of the integration.

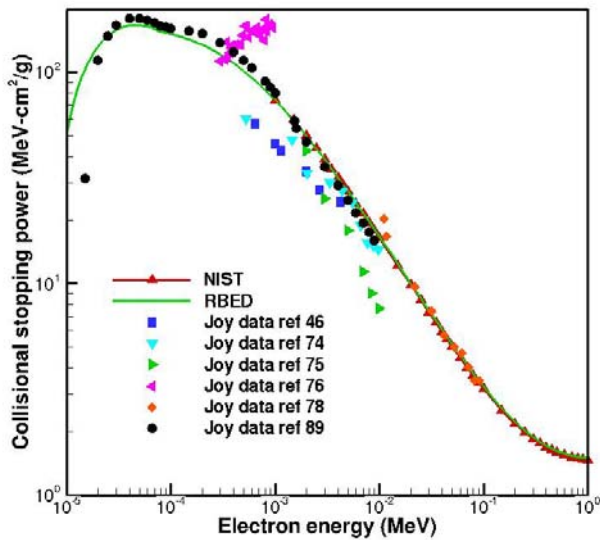


Fig. 2a. Comparison of Al stopping power computed from RBED differential scattering cross section with NIST and experimental values.

Fig. 2b. shows a similar comparison for gold. Agreement for gold with the Joy Ref. 47 data is very good for energies down to 1 keV and tolerable below for energies below 1 keV. Without error bars on the experimental values, it is difficult to say whether the differences are due to model uncertainty, experimental uncertainty or both.

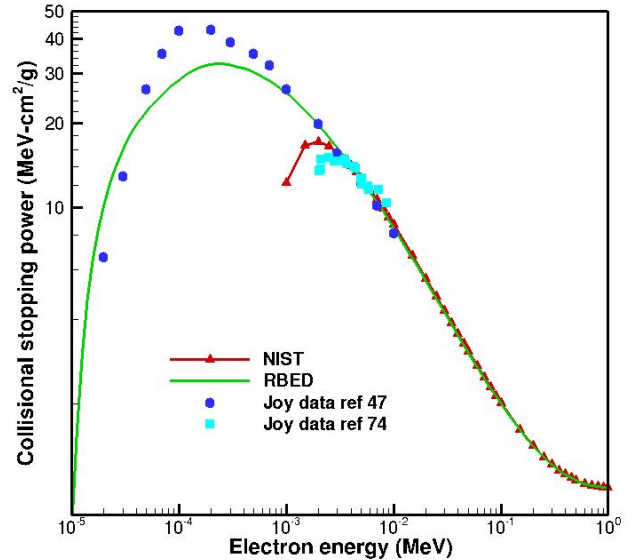


Fig. 2b. Comparison of Au stopping power computed from RBED differential scattering cross section with NIST and experimental values.

#### IV. MMS RESULTS

Several MMS test problems are presented in this section to investigate the utility of the energy-FE-weighted cross sections. In the first MMS test problem, standard MG cross sections and stopping powers, computed by using a step-discontinuous energy basis, are utilized. A simple MMS angular flux solution is used that is expected to provide a numerically “exact” solution (to within round-off and iterative convergence errors). The test geometry consists of two regions (gold-aluminum) in one spatial dimension, with cross sections and stopping powers obtained from the RBED scattering kernel.

The second test problem uses energy-FE-weighted cross sections computed from linear energy bases. The MMS angular flux solution is 7<sup>th</sup>-order in angle, designed to test scattering moments up to 7<sup>th</sup> order. Like the previous test problem, this test problem uses the RBED scattering kernel and should provide numerically exact solutions. The third and final test problem utilizes a simpler scattering kernel so that an analytic MMS source term may be computed. This test problem is designed to be exactly representable in space and angle, but not in energy, so that the solution convergence with energy-mesh refinement can be investigated.

## 1. Numerically Exact Test Problem Using RBED MG Cross Sections

In this test problem, standard MG cross sections are utilized, computed by using step-discontinuous energy basis functions. The spatial geometry is two-region aluminum-gold in one spatial dimension. Electrons with maximum energy of 1 MeV are modeled using 40 uniform energy elements,  $S_N$  angular treatment using  $S_8$  angular quadrature, DFE-spatial discretization and  $P_1$  scattering. Energy-FE scattering cross sections are computed from Eq. (11b) using step energy basis, using an adaptive integration routine to evaluate the energy integrals. Group-average restricted stopping powers are computed from Eq. (14), also using an adaptive integration routine. A maximum energy loss of 20 keV is used to demark the CSD and MG-Legendre treatments.

The MMS solution for this test problem is

$$\psi_{MMS}(x, \mu, E) = x(1 + \mu)E, \quad (15a)$$

and the corresponding MMS fixed source is

$$Q_{MMS}(x, \mu, E) = (\mu + x\sigma_{t,g})(1 + \mu)E - x(1 + \mu)S_{R,g} - xE(\sigma_{0,g} + 3\mu\sigma_{1,g}), \quad E \in [E_{g,l}, E_{g,u}], \quad (15b)$$

where  $E_{g,l}$  and  $E_{g,u}$  are the lower- and upper-energy bounds of energy element  $g$ .

For each energy element, a linear system is constructed from the spatial and angular discretization of the Boltzmann-CSD equation, which is solved iteratively with a GMRES algorithm with a convergence tolerance of  $10^{-12}$ . The maximum relative and absolute error norms over all of the energy elements are listed in Table I. The error norms are near the convergence tolerance of the GMRES iterations, indicating that the algorithm has been implemented correctly.

Table I. Max error norms of test problem 1

Error metric	$L_2$ error norm
Absolute	$9.85 \times 10^{-11}$
Relative	$1.97 \times 10^{-10}$

## 2. Numerically Exact Test Problem Using RBED FE-Weighted Cross Sections

In this section, energy-FE weighted cross sections using linear energy basis functions from the RBED scattering kernel are utilized. Cross sections are computed for electrons with a maximum energy of 1 MeV in aluminum, with a logarithmic energy mesh, including 10 energy elements. A scattering cosine of  $\mu_0=0.99$  is used to demark the CSD and MG-Legendre treatments, with scattering events with scattering cosines greater than  $\mu_0$  included in the restricted stopping power and those with scattering cosines less than  $\mu_0$  included in the catastrophic scattering.

The MMS angular flux solution is linear in space and energy, and 7<sup>th</sup>-order in angle, in order to test scattering cross section moments up to 7<sup>th</sup> order. The angular dependence of the MMS angular flux is shown in Fig. 3.

$$\psi_{MMS}(x, \mu, E) = xE \sum_{n=0}^7 \mu^n. \quad (16a)$$

The angular dependence of the MMS angular flux solution is shown in Fig. 3.

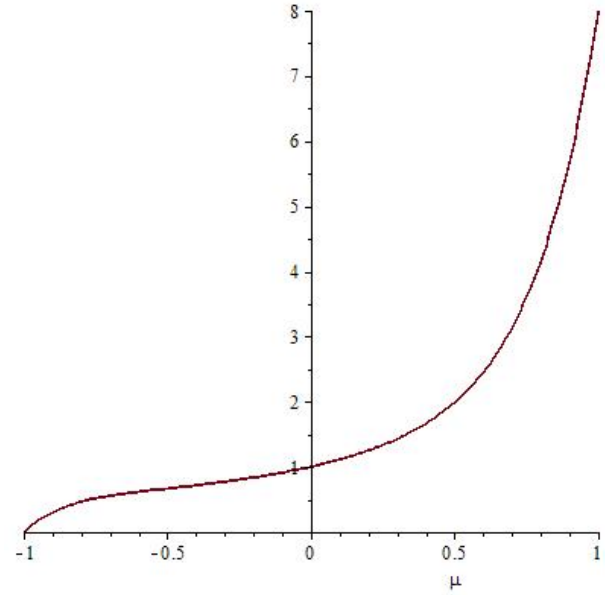


Fig. 3. Angular dependence of the MMS angular flux solution for test problem 2.

The MMS source term for this test problem is fairly complicated, and has been computed by Maple [8] and is given in Eq. (16b),

$$Q_{MMS}(x, \mu, E) = [\mu E + xE\langle\sigma_t\rangle + xE\langle S_R\rangle + xE^u S_R^u - xE^l S_R^l] \sum_{n=0}^7 \mu^n - xE \left[ \frac{176}{105} \langle\sigma_{s,0}\rangle + \frac{248}{105} \mu \langle\sigma_{s,1}\rangle + \left( \frac{18}{7} \mu^2 - \frac{6}{7} \right) \langle\sigma_{s,2}\rangle + \left( \frac{314}{99} \mu^3 - \frac{314}{165} \mu \right) \langle\sigma_{s,3}\rangle + \left( \frac{26}{11} \mu^4 - \frac{156}{77} \mu^2 + \frac{78}{385} \right) \langle\sigma_{s,4}\rangle + \left( \frac{34}{13} \mu^5 - \frac{340}{117} \mu^3 + \frac{170}{273} \mu \right) \langle\sigma_{s,5}\rangle + \left( \mu^6 - \frac{15}{11} \mu^4 + \frac{5}{11} \mu^2 - \frac{5}{231} \right) \langle\sigma_{s,6}\rangle + \left( \mu^7 - \frac{21}{13} \mu^5 + \frac{105}{143} \mu^3 - \frac{35}{429} \mu \right) \langle\sigma_{s,7}\rangle \right]. \quad (16b)$$

The angle brackets  $\langle \rangle$  indicate energy-FE weighted stopping-power and cross-section values.

A linear system is constructed by using an  $S_N$  angular treatment with  $S_{16}$  quadrature, DFE spatial differencing and

DFE energy differencing, resulting in a linear system for each energy element. The linear systems for each energy element are solved successively using a GMRES iterative algorithm. The convergence tolerance of the GMRES iterations is  $10^{-12}$ . Table II lists the global error norms for this test problem, which are near the convergence tolerance specified for the GMRES iterations, indicating that the algorithm is implemented correctly.

Table II. Error norms of test problem 2.

Error Metric	$L_2$ Error Norm
Absolute	$4.28 \times 10^{-12}$
Relative	$1.02 \times 10^{-11}$

### 3. Numerically Inexact Test Problem Using Energy-FE Weighted Cross Sections from a Simpler Scattering Kernel

This test problem makes use of a simpler scattering kernel than the RBED model, in order to facilitate the analytic computation of an MMS source term. In order to mimic electron scattering, a cross section kernel is desired that is highly forward peaked and large for small energy transfers. Eq. (17) shows a differential scattering cross section with these properties,

$$\sigma_s(\mu_0, E \rightarrow E') = \frac{\delta[\mu_0 - (1 - E + E')]}{E + \varepsilon - E'}, \quad E > E', \quad (17)$$

where  $\varepsilon$  is a small parameter chosen to tune the gradient of the function for small energy loss. The energy dependence of the scattering kernel is shown in Fig. 4. for  $\varepsilon=0.01$ .

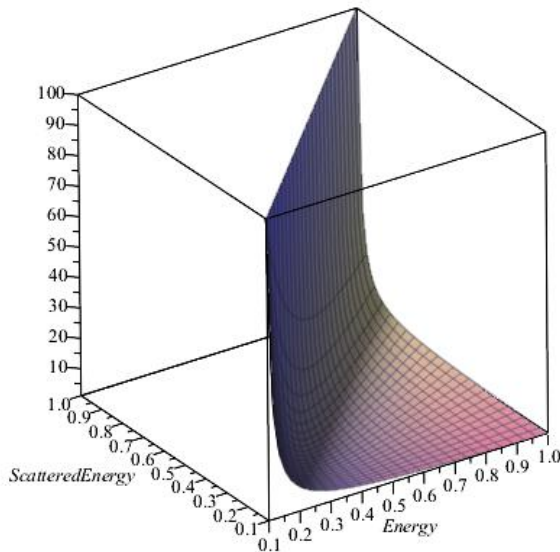


Fig. 4. Scattering kernel for test problem 3 for  $\varepsilon=0.01$ .

The total cross section is for this scattering kernel is given by

$$\sigma_t(E) = \int_{E_{cut}}^E \frac{dE'}{E + \varepsilon - E'} = \ln\left(\frac{E + \varepsilon - E_{cut}}{\varepsilon}\right), \quad (18)$$

where  $E_{cut}$  is the lower-energy cutoff. The scattering moments are given by

$$\sigma_s^l(E' \rightarrow E) = \frac{P_l(1 - E' + E)}{E' + \varepsilon - E}. \quad (19)$$

For this scattering kernel, the MMS source term is given by

$$Q_{MMS}(x, \mu, E) = \mu \frac{\partial \psi_{MMS}}{\partial x} + \sigma_t(E) \psi_{MMS}(x, \mu, E) - \sum_{l=0}^L \frac{2l+1}{2} P_l(\mu) \int_{-1}^1 P_l(\mu') \int_E^{E_{max}} \frac{P_l(1 - E' + E)}{E' + \varepsilon - E} \psi_{MMS}(x, \mu', E') d\mu' dE', \quad (20)$$

where  $E_{max}$  is the maximum energy. For an MMS angular-flux solution of

$$\psi_{MMS}(x, \mu, E) = \frac{x(1 + \mu)}{E} \quad (21)$$

the MMS source term may be computed analytically,

$$Q_{MMS}(x, \mu, E) = \ln\left(\frac{E + \varepsilon - E_{cut}}{\varepsilon}\right) \frac{x(1 + \mu)}{E} - \frac{\mu(1 + \mu)}{E} - \ln\left[\frac{E}{E_{max}} \frac{E_{max} + \varepsilon - E}{\varepsilon}\right] \frac{x}{E - \varepsilon} - \frac{x\mu}{E - \varepsilon} \left[ (E + 1) \ln\left(\frac{E}{E_{max}}\right) + (1 + \varepsilon) \ln\left(\frac{E_{max} + \varepsilon - E}{\varepsilon}\right) \right]. \quad (22)$$

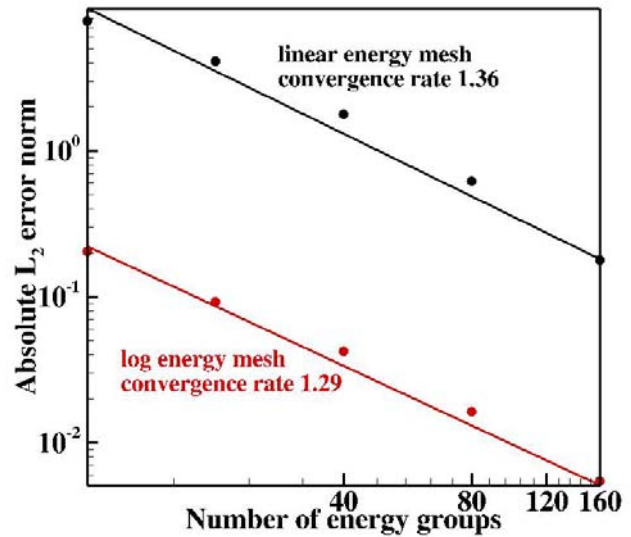


Fig. 5. Convergence of error with energy-mesh refinement.

For a value of  $\varepsilon$  of 0.01 MeV, an upper energy  $E_{max}=1$  MeV, and a lower-energy cutoff,  $E_{cut}=20$  keV,  $S_8$  angular quadrature, and DFE energy and spatial approximation, the

numerical angular flux solution is obtained with a GMRES algorithm. The error norms as a function of number of energy elements is shown in Fig. 5. Results are shown for both a linear energy mesh and for a logarithmically-distributed energy mesh. For a linear energy mesh, most of the error is from the lowest-energy group. Using a logarithmically-distributed energy mesh, substantially reduces the error norm, as shown in Fig. 5. The convergence rates for the linear and log mesh results are 1.36 and 1.29, respectively, somewhat less than the order-2 convergence rate expected for energy-DFE discretization with linear basis functions.

## V. SUMMARY AND COMMENTS

The evaluation and application of energy-FE weighted scattering cross sections has been described. A particular form of the electron inelastic scattering kernel, the RBED formula, has been used to compute stopping powers and cross sections for an energy-DFE discretization of electron-scattering cross sections for electron transport applications. Stopping powers computed with the RBED formula have been compared to experimental values for two elements, aluminum and gold. Comparison with additional elements would be enlightening. The computed stopping-power values are sensitive to the limits of integration used, and this behavior could be investigated further. Furthermore, since the error information on the measured stopping powers tend to be lacking, further evaluation of the stopping power data is in order.

Applying both MG and energy-FE weighted cross sections to MMS test problems shows that basically "exact" results may be obtained for MMS test problems where the algorithm should be able to exactly model the problem parameters. Furthermore, a test problem that is not exactly modelable shows convergence with energy-mesh refinement, though with a convergence rate less than the expected value of two.

The partition between a Boltzmann treatment and a CSD treatment is determined either by specifying an energy-loss value of a scattering cosine value to demark the two treatments. It would be instructive to attempt to determine optimal values of this partition, providing the most accurate possible results. Furthermore, the relationship between the CSD term and the  $\delta$ -function down-scatter term could be investigated. Both terms decrease energy without direction change, but are numerically very different.

For simplicity, all of the test problems considered here are one dimensional in the spatial variable, and it would be instructive to test the energy-FE weighted cross sections in some two- and three-dimensional test problems. Also, the test problems considered here used linear energy basis functions, and it would be interesting to use quadratic energy basis functions, and determine convergence rates with energy mesh refinement.

In this work, only the electron inelastic scattering was considered. In order to generate useful electron scattering

cross all of the electron physics will need to be considered, include electron elastic scattering. The Fokker-Planck (FP) angular redistribution term has been neglected in this work. This term is thought to be small, but could be investigated for the elastic scattering cross sections.

## ENDNOTES

<sup>a</sup>Sandia National Laboratories is a multi-mission laboratory managed and operated by Sandia Corporation, a wholly owned subsidiary of Lockheed Martin Corporation, for the U.S. Department of Energy's National Nuclear Security Administration under contract DE-AC04-94AL85000.

## REFERENCES

1. L. J. LORENCE, Jr., J. E. MOREL and G. D VALDEZ, "Physics Guide to CEPXS: A Multigroup Coupled Electron-Photon Cross-Section Generating Code Version 1.0," SAND89-1685 Sandia National Laboratories (1985).
2. J. E. MOREL, "Fokker-Planck Calculations Using Standard Discrete Ordinates Transport Codes," *Nucl. Sci. Eng.* **79**, 340-356 (1981).
3. C. DRUMM, W. FAN and S. PAUTZ, "Phase-Space Finite Elements in a Least-Squares Solution of the Transport Equation," *Proc. M&C 2013*, Sun Valley, Idaho, May 5-9, 2013, American Nuclear Society (2013).
4. C. R. DRUMM, W. C. FAN, L. LORENCE and J. LISCUM-POWELL, "An analysis of the extended-transport correction with application to electron beam transport," *Nucl. Sci. Eng.* **155**, 355-366 (2007).
5. Y-K. KIM, J. P. SANTOS and F PARENTE, "Extension of the binary-encounter-dipole model to relativistic incident electrons," *Phys. Rev. A*, **62**, 1-14 (2000).
6. D.E. CULLEN, et al., "Tables and Graphs of Atomic Subshell and Relaxation Data Derived from the LLNL Evaluated Atomic Data Library (EADL), Z = 1 - 100," Lawrence Livermore National Laboratory, UCRL-50400, Vol. 30, October 1991.
7. ESTAR "Stopping power and range tables for electrons," National Institute of Standards and Technology, <http://physics.nist.gov/PhysRefData/Star/Text/ESTAR.html>
8. D. C. JOY, "A Database of Electron-Solid Interactions," ORNL report, Rev. 08-1, Oak Ridge National Laboratory (2008).
9. Maple 18. Maplesoft, a division of Waterloo Maple Inc., Waterloo, Ontario.